Neutron powder-diffraction studies of lithium, sodium, and potassium metal

R. Berliner and O. Fajen
Research Reactor and Department of Physics, University of Missouri–Columbia, Columbia, Missouri 65211

H. G. Smith
Solid State Division, Oak Ridge National Laboratory, Oak Ridge, Tennessee 37830

R. L. Hitterman
Intense Pulsed Neutron Source, Argonne National Laboratory, 9700 South Cass Avenue, Argonne, Illinois 60439
(Received 30 May 1989; revised manuscript received 30 August 1989)

Neutron powder-diffraction measurements have been performed on polycrystalline lithium and sodium specimens at 80 and 20 K and on potassium metal at 80 and 10 K. Lithium is bcc (body-centered cubic) at room temperature and undergoes a martensitic structural phase transformation to a 9*R* (samarium-type) form at low temperature. This experiment presents evidence that the 9*R* phase is present in sodium as well as lithium. No evidence of a transformation was observed in potassium at 10 K. The diffraction lines for both lithium and sodium after the phase transformation exhibit position shifts and broadening characteristic of stacking-fault defects. The line shifts, line broadening, and transformed fraction for the low-temperature phase of lithium and sodium metal are reported. The diffraction peak position shifts are, however, different from those predicted for deformation-type stacking faults alone. Qualitative agreement of the experimental results with stacking-fault-model calculations was obtained for a "double-twin" type of layer defect.

I. INTRODUCTION

Barrett and co-workers[1,2] were the first to study the alkali metals at low temperature with x-ray diffraction. They discovered that lithium and sodium undergo spontaneous structural phase transformations from the high-temperature body-centered-cubic (bcc) structure to hexagonal forms at low temperature. In lithium, below the martensitic transformation temperature $T_m \sim 77$ K, the structure was identified as a mixture of hexagonal-close-packed (hcp) material coexistent with a substantial fraction of the untransformed bcc phase. Some of the material could be converted to the face-centered-cubic (fcc) form by cold work. In sodium, below $T_m \sim 35$ K, the structure was found to be a combination of hcp and bcc material. In both cases, the diffraction lines were affected by a high density of stacking faults, and the transformation temperature, transformed fraction, low-temperature structure, and reverse-transformation temperature were found to be affected by cold work. Barrett found no evidence of a structural phase transformation in potassium.

Later neutron-scattering experiments in lithium by McCarthy *et al.*[3] produced diffraction patterns which were interpreted by Overhauser[4] as evidence that the low-temperature phase was really a hexagonal polytype, similar to the structure adopted by samarium metal,[5] the 9*R*. As a hcp lattice is composed of alternating layers stacked *ABAB* . . . in the *c* direction and a fcc lattice is denoted by the stacking sequence *ABCABC* . . . , the 9*R* polytype is constructed from the 9-layer stacking sequence *ABCBCACAB* . . . . Quantitative structural analysis of the data of Ref. 3 was not possible due to preferred orientation effects in the sample and interference caused by diffraction from the aluminum sample can.

Neutron powder-diffraction measurements on polycrystalline lithium metal by Berliner and Werner[6] demonstrated that the low-temperature lithium structure was indeed 9*R*, but that the diffraction-line peak positions were shifted and the linewidths broadened by a high density of stacking-fault defects in the planes perpendicular to the *c* axis. They were able to show, by a detailed analysis of the effect of stacking faults on diffraction, that the observed effects could be explained by the random occurrence of deformation-type stacking faults predominantly at certain types of sites in the stacking order. However, recent neutron-diffraction measurements on lithium single crystals by Smith[7] and Smith and Berliner[8] obtained peak shifts at variance with the predictions of this model. Investigation of these differences, which were too small to be seen in previous powder-diffraction work, was the initial motivation for this experiment. In addition, preliminary powder-diffraction data from sodium metal suggested the presence of the 9*R* phase, but the low resolution of the data precluded quantitative analysis of the peak shifts or conclusive verification of the 9*R* phase.

II. EXPERIMENTAL RESULTS

In order to minimize the effect of preferred orientation and coarse-grain size, the samples for this experiment were in the form of 1-mm-diam wires. The wire was extruded in a helium atmosphere, rolled loosely into small balls, and immediately packed and sealed into 1-cm diam vanadium sample cans. Two samples of each metal were prepared. The ^{7}Li for the lithium specimens was taken from the same material used for specimens by McCarthy *et al.*[3] and by Berliner and Werner.[6] The sodium and potassium metal were obtained at 99.95% purity packed in

 ©1989 The American Physical Society

argon gas.[9]

The neutron powder-diffraction experiments were performed on the general-purpose powder diffractometer (GPPD) at the Intense Pulsed Neutron Source (IPNS) at Argonne National Laboratory.[10] Specimen temperatures were monitored by a thermometer mounted on the cryorefrigerator cold tip just above the sample-mounting flange.

Data from neutron powder diffraction on two lithium specimens and two sodium specimens were obtained at 80 and 20 K. The diffraction patterns from one of our lithium specimens, at 80 K, before the martensitic transformation, and at 20 K, after the transformation, are shown in Figs. 1(a) and 1(b). Similar data for sodium metal are shown in Figs. 2(a) and 2(b). The vertical scales of the figures were chosen to illuminate the small diffraction peaks of the new phase while the horizontal scales are presented in terms of d spacing. A comparison of the monitor-normalized diffraction data at 20 and 80 K for both metals showed no evidence of transformation-induced diffuse scattering.

Lattice parameters derived from the data were used to calculate the diffraction-line positions for the bcc and 9R crystal structures which are marked on the figures. In

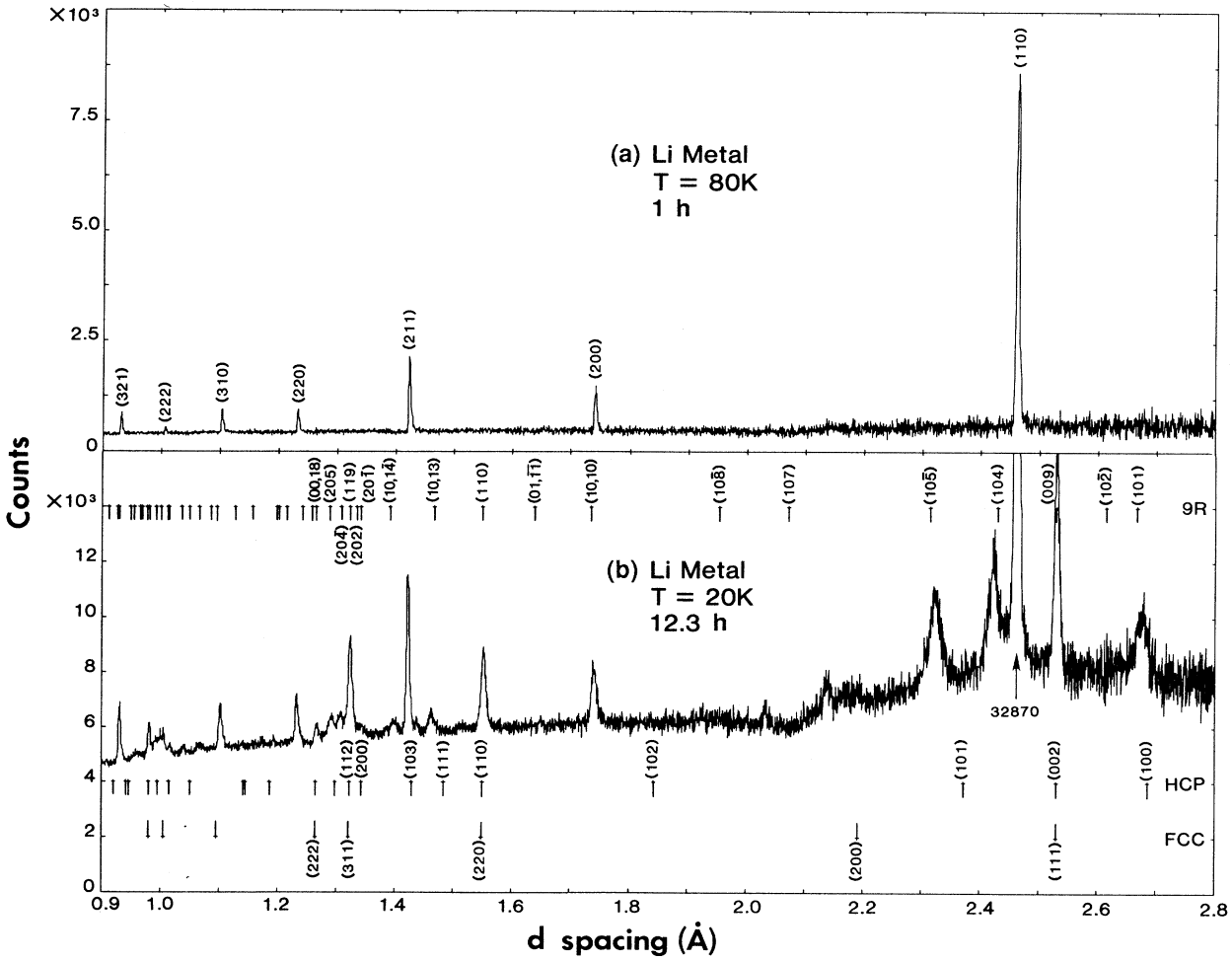

FIG. 1. Neutron time-of-flight diffraction data for lithium metal. The data are the sum of the left and right 148° detector banks on the GPPD at IPNS. The raw time-of-flight data have been normalized to the variation in the incident-beam spectrum and converted to d spacing. (a) Lithium metal above the martensitic transformation at 80 K: 2 h. (b) Lithium metal after the martensitic transformation at 20 K: 12.5 h. The scale of the figure was chosen to show the detail of the small diffraction peaks present after the transformation. The peak intensity for those peaks that are off-scale is noted on the figure. The position and indices for the 9R-, bcc-, hcp-, and fcc-phase diffraction peaks have been marked.

TABLE I. Measured bcc and $9R$-phase lattice parameters for lithium and sodium metal at 20 K. The hexagonal-phase-transformed fraction and the difference in atomic volume between the $9R$ and bcc phases are also listed. The results for lithium obtained by Berliner and Werner (Ref. 6) are shown for comparison.

	bcc	$9R$			
	a	a	c	f	$V_{9R}-V_{bcc}$
Lithium	3.478 51(1)	3.1010(3)	22.7649(2)	0.66	0.019(4) Å^3
Ref. 6	3.4769(3)	3.0986(3)	22.735(3)	0.698	0.011(5) Å^3
Sodium	4.221 40(2)	3.765 86(8)	27.6531(2)	0.43	0.123(6) Å^3

addition, the positions of the diffraction lines for the polytype fcc and hcp structures are also noted. The lattice parameters for the bcc and hexagonal phases, atomic volumes, and transformed fractions following the martensitic transformation are collected for both metals in Table I. The values obtained by Berliner and Werner[6] for lithium metal are listed for comparison.

The general structure of the diffraction patterns after the transformation is as has been previously described for lithium metal:[6] the strongest peaks conform to the

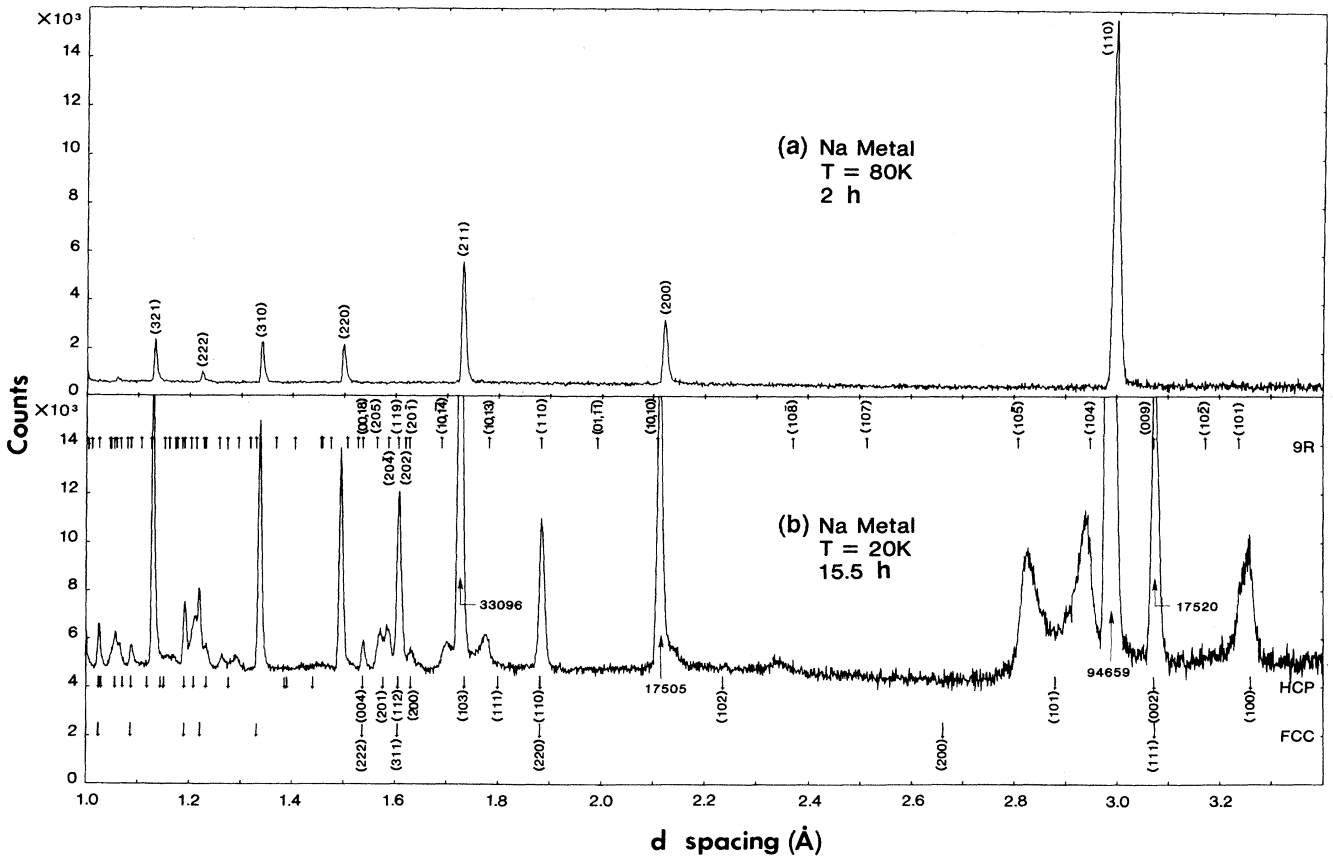

FIG. 2. Neutron time-of-flight diffraction data for sodium metal. The data are the sum of the left and right 90° detector banks on the GPPD at IPNS. The raw time-of-flight data have been normalized to the variation in the incident-beam spectrum and converted to d spacing. (a) Sodium metal above the martensitic transformation at 80 K: 2h. (b) Sodium metal after the martensitic transformation at 20 K: 15.4 h. The scale of the figure was chosen to show the detail of the small diffraction peaks present after the transformation. The peak intensity for those peaks that are off-scale is noted on the figure. The position and indices for the $9R$-, bcc-, hcp-, and fcc-phase diffraction peaks have been marked.

TABLE II. Measured diffraction peak positions, integrated intensities, and diffraction peak widths for lithium metal at 20 K. Only those peaks that can be unambiguously identified and separated from interference are listed. The table has been ordered by d spacing and the diffraction peaks identified with their bcc-phase or 9R-phase Miller indices. The shift of the stacking-fault-affected 9R-phase lines is shown by the nonintegral values of the Miller index l, calculated as described in the text. The diffraction peak widths, converted to angstroms, are listed in the table. The peak width for stacking-fault-affected lines, corrected for the instrumental resolution and projected onto a $[h0l]$ reciprocal-lattice line, are listed in units of l in the table. The uncertainties in the integrated intensity, measured diffraction peak position, Miller index l, and FWHM are obtained from the least-squares peak fits as described in the text and do not reflect systematic errors. (a) Lithium metal: Note that the bcc-(200) peak, although visible, cannot be separated from the 9R-(1,0,10) and has been listed as unresolved. (b) Sodium metal: Data for peaks for the hcp phase are also shown. The hcp-phase lines use 9R indexing as described in the text.

(a)

bcc $h\,k\,l$	9R $h\,k\,l$	d meas. (Å)	l	Δl	FWHM (10^3 Å)	Projected FWHM	$10^{-5}I$
	1 0 1	2.673 92±0.000 12	0.831±0.004	−0.169±0.004	22.68±0.32	0.691±0.010	5.21±0.07
	0 0 9	2.529 43±0.000 02			7.34±0.06		8.70±0.05
1 1 0		2.459 68±0.000 01			7.61±0.03		24.43±0.05
	1 0 4	2.423 14±0.000 08	4.059±0.001	0.059±0.001	21.75±0.22	0.183±0.002	9.78±0.08
	1 0 $\bar{5}$	2.321 38±0.000 09	−4.934±0.001	0.066±0.001	24.99±0.24	0.201±0.002	8.15±0.08
	1 0 $\bar{8}$	not observed					
2 0 0		not resolved					
	1 0 10	not resolved					
	1 1 0	1.551 21±0.000 05			8.46±0.15		2.97±0.04
	1 0 13	1.461 52±0.000 29	13.070±0.004	0.070±0.004	10.39±1.10	0.112±0.13	0.81±0.10
2 1 1		1.420 00±0.000 02			4.22±0.08		3.99±0.04
	1 0 $\overline{14}$	1.396 75±0.000 43	−13.922±0.006	0.078±0.006	10.52±1.40	0.124±0.019	0.48±0.07
	1 1 9	1.322 01±0.000 04	8.997±0.00	0.000	6.87±0.12		2.63±0.11
	2 0 $\bar{4}$	1.305 41±0.000 26	−4.118±0.015	−0.118±0.015	11.42±0.83	0.544±0.037	1.08±0.06
	2 0 5	1.288 80±0.000 29	4.984±0.014	−0.016±0.014	12.29±0.75	0.578±0.047	1.12±0.06
	0 0 18	1.265 55±0.000 17			4.99±0.53		0.45±0.03
2 2 0		1.230 67±0.000 12			3.29±0.47		0.82±0.15
3 1 0		1.099 46±0.000 07			4.87±0.21		1.17±0.03

(b)

bcc $h\,k\,l$	9R $h\,k\,l$	hcp $h\,k\,l$	d meas. (Å)	l	Δl	FWHM (10^3 Å)	Projected FWHM	$10^{-5}I$
		1 0 0	3.257 69±0.000 19	0.401±0.011	0.401±0.011	9.46±0.65		1.59±0.13
	1 0 1		3.247 13±0.000 23	0.749±0.007	−0.206±0.006	30.10±0.22	0.781±0.009	9.30±0.02
	0 0 9		3.072 57±0.000 03			12.50±0.07		15.25±0.06
1 1 0			2.984 98±0.000 01			11.72±0.02		106.55±0.11
	1 0 4		2.937 14±0.000 29	4.092±0.002	0.092±0.002	16.99±0.52	0.098±0.004	5.77±0.47
		1 0 $\overline{4.5}$	2.919 13±0.001 70	4.224±0.012	0.276±0.012	34.47±3.40	0.230±0.024	4.10±0.55
		1 0 4.5	2.843 96±0.002 30	4.759±0.016	0.259±0.016	28.88±2.60	0.196±0.019	5.08±0.76
	1 0 $\bar{5}$		2.820 97±0.000 48	4.919±0.003	0.081±0.003	22.97±0.65	0.143±0.005	7.48±0.71
	1 0 $\bar{8}$		2.340 77±0.000 88	8.226±0.006	−0.226±0.006	29.40±2.60	0.204±0.109	1.02±0.10
	1 0 10		2.136 39±0.000 49	9.780±0.004	−0.220±0.004	23.94±1.60	0.182±0.013	1.46±0.08
2 0 0			2.111 54±0.000 03			9.20±0.07		12.41±0.06
	1 1 0		1.882 93±0.000 04			9.00±0.10		5.79±0.04
	1 0 13		1.769 24±0.000 22	13.13±0.002	0.130±0.002	23.87±0.65	0.243±0.068	3.02±0.07
2 1 1			1.723 89±0.000 01			6.84±0.03		22.52±0.06
	1 0 $\overline{14}$		1.700 91±0.000 29	13.870±0.003	0.130±0.003	21.33±0.91	0.230±0.010	2.19±0.09
	2 0 1		1.629 47±0.000 26	0.650±0.071	0.350±0.071	10.28±0.78	2.340±0.210	0.73±0.04
	1 1 9		1.605 86±0.000 03			7.72±0.09		6.07±0.04
	2 0 $\bar{4}$		1.583 50±0.000 23	4.170±0.011	−0.170±0.011	12.23±0.65	0.506±0.030	1.87±0.07
	2 0 5		1.567 97±0.000 23	4.843±0.010	−0.157±0.010	10.15±0.65	0.352±0.027	1.47±0.08
	0 0 18		1.536 28±0.000 13			5.20±0.39		0.76±0.04
2 2 0			1.492 80±0.000 03			5.63±0.07		6.24±0.04
3 1 0			1.335 63±0.000 03			5.54±0.5		6.81±0.04

diffraction pattern expected from the $9R$ lattice structure with some peaks shifted from their calculated positions and substantially broadened. A large fraction of both metals remains in the bcc form. In the absence of a detailed model for the distortions imposed on the diffraction pattern at low temperature by the defect structure, the diffraction-line intensities, widths, and positions were determined in a model-independent fashion. Least-squares fits to the peaks in the diffraction data were performed by first normalizing the spectra to the variation in the incident-beam intensity as a function of neutron time of flight (TOF) using the TOF parameter values appropriate to the IPNS target-moderator configuration. Separate regions of the data were then fitted, as a function of TOF, using the eight-parameter peak shape function[11,12] to obtain the peak position, integrated intensity, and peak width for the individual diffraction lines.

Table II contains the results of a series of these least-squares fits to the peaks observed in the diffraction patterns of lithium and sodium metal below the martensitic transformation. In the region above 1.25 Å in lithium and 1.5 Å for sodium, it is possible to fit most of the bcc-phase diffraction lines and the majority of the strong peaks attributed to the $9R$ structure. The position and width of each of the diffraction lines in the 20-K diffraction pattern is given in Table II in terms of its measured d spacing. The diffraction peak positions, peak position shifts, and linewidths are also tabulated in terms of their reciprocal-space coordinates. This portion of the table will be discussed in Sec. III below. The integrated intensity of each of the diffraction peaks is also noted. In lithium metal, the broad feature near 2.2 Å is consistent with the presence of a small fcc-phase fraction as has been observed in single-crystal experiments.[7,8] The two small peaks in the 20-K diffraction pattern near 2.02 and 2.14 Å are uncorrelated with any of the structures discussed above and are believed to be contamination.

In sodium metal, close inspection of the (104) and (10$\bar{5}$) $9R$ diffraction peaks shows evidence of additional broadening that may be due to the contribution of a hcp phase. Neutron-diffraction investigations of single-crystal sodium specimens below the martensitic transformation indicate the presence of a hcp-phase fraction in addition to the bcc and $9R$ phases.[13] This is in contrast to the results of lithium single-crystal diffraction experiments where a hcp phase has not been observed. The effect here is much less pronounced than in the case of the single-crystal experiments, but we have analyzed $9R$-(101), $9R$-(104), and $9R$-(10$\bar{5}$) assuming the presence of a hcp phase.

The transformed fractions for both metals were estimated on the basis of the ratio between the bcc-(110) integrated intensity and that of the $9R$-(009). These two diffraction lines are very close together in TOF and we have ignored any difference in thermal factors.

Neutron-diffraction data on potassium metal were obtained for one specimen at 80 and 10 K. The structure at 10 K remains bcc with $a = 5.2334 \pm 0.0001$ Å. Examination of data in the region of the bcc-(110) diffraction peak revealed no evidence of another phase. We estimate that we would be able to observe any hexagonal polytype in potassium with a phase fraction at 10 K greater than 4%. Unpublished data from neutron-diffraction experiments on a highly perfect single-crystal potassium specimen place still-lower limits on the possible transformed fraction [less than $(4 \times 10^{-3})\%$].[14]

III. DISCUSSION

A. Experimental line shifts and linewidths

Neutron-diffraction experiments on single crystals of lithium and sodium metal after the martensitic transformation have confirmed the conclusions drawn from the earlier powder-diffraction experiments on lithium metal.[6-8] Diffraction lines with Miller indices h, k, and l such that $h - k = 3n \pm 1$, are found to be shifted away from their ideal positions and broadened. The single-crystal experiments show that the diffraction peak position shifts and line broadening are completely confined to displacements in reciprocal space parallel to the c^* axis. These effects are the signature of diffraction from hexagonal polytypes with basal-plane layer disorder.

When this experiment is interpreted in light of the single-crystal investigations, indexing of the $9R$ powder pattern gives fractional values of the index l. The indices and the observed displacements of reflections with $h - k = 3n \pm 1$ are given in Table II. In like manner, the substantial broadening that is observed for the stacking-fault-affected lines is interpreted as a smearing of the diffracted intensity distribution parallel to the c^* axis.

The $R\bar{3}M$ symmetry of the $9R$ crystal structure assures that diffraction peaks are observed only for $-h + k + l = 3n$ with n an integer. Equivalent reflections are produced by the positive and negative values of n. In this manner, the (015) and (10$\bar{5}$) are equivalent as are the (01$\bar{4}$) and (104). We will discuss the peak position shifts in reciprocal space along the [10l] and [20l] reciprocal-lattice lines and have used these equivalent Miller-index designations as appropriate.

The $\{hhl\}$ and $\{h0l\}$ planes for the ideal $9R$-phase reciprocal lattice of lithium and sodium metal below the martensitic transformation are displayed in Fig. 3. The diagram for the $9R$ phase of lithium metal is essentially the same except that the quality of the data did not permit the analysis of as many of the $9R$-phase diffraction lines. The reciprocal-lattice spots corresponding to the hcp reflections in sodium have not been plotted but would appear near (1 0 4.5), (1 0 $\bar{4}$.5), and (100) when $9R$ indexing is used.

Only a few of the $9R$ peaks can be unambiguously identified and their l shifts determined, but the pattern of diffraction-line displacements is interesting. The (104) and (10$\bar{5}$) peaks and the (1 0 13)-(1 0 $\overline{14}$) pair, along with the (20$\bar{4}$) and (205) pair, have the same structure factor ($F^2 = 57.74b^2$) and evidence the same l-shift direction in both metals. The peaks lying along the reciprocal-lattice [10l] lines are shifted in the $+l$ direction. Those lying along the [20l] are shifted in the opposite direction. Taken alone and ignoring momentarily the relative magnitudes of the displacements, this shift pattern is consistent with the presence of $H \wedge K$ (deformation) stacking faults

as was shown in Ref. 6.

The $9R$-(101), $9R$-(1 0 10), $9R$-(10$\bar{8}$) and $9R$-(20$\bar{1}$) form a second family of peaks, all having the same structure factor ($F^2=16.34b^2$), that are identified in the diffraction patterns. Only the (101) is clearly resolved in lithium and it shifts in a direction opposite to the shift of the (104). In sodium metal, the "contrary" shift of the (101) is observed once again. In addition, the (1 0 10) and (10$\bar{8}$) shift in the $-l$ direction. The (201) peak is observed to shift in the direction opposite to the shift of the (205) and (20$\bar{4}$). Finally, the $9R$-(10$\bar{2}$) and $9R$-(107) lines, having the smallest structure factor, $F^2=6.96b^2$, are not observed in our diffraction data and were not clearly observed in the previous powder-diffraction experiments on lithium.[6]

These observations confirm the earlier reports[7,8] of the peak position shifts in neutron-diffraction experiments on single-crystal lithium specimens. Deformation faults, however, cause $9R$-(101)- and $9R$-(104)-type peaks to shift in the same direction by approximately the same amount.[6] Only when some of the smaller $9R$-phase diffraction lines can be clearly resolved, as in this study and in the single-crystal experiments, does it become clear that deformation-type stacking faults alone cannot account for the diffraction data. This experiment also shows that the puzzling shifts in the diffraction-line positions are intrinsic and not due to the presumably differing defect densities of an extruded wire and a well-annealed single crystal.

In sodium, the hcp-phase (101) and (10$\bar{1}$) diffraction peaks are very close in TOF to the stacking-fault broadened $9R$-phase (104) and (10$\bar{5}$) lines, making the analysis difficult. The least-squares fits show the hcp-(100) as essentially unbroadened, but considerably shifted from its ideal position. The hcp-(101) and hcp-(10$\bar{1}$) appear displaced from their ideal locations and have substantially broadened diffraction peak widths. The latter observation is in qualitative agreement with the results of the subsequently performed sodium single-crystal neutron-diffraction experiments.[13]

The measured widths of the lithium diffraction lines at 80 and at 20 K are shown in Fig. 4(a). Similar data for sodium metal are shown in Fig. 4(b). The linewidths have

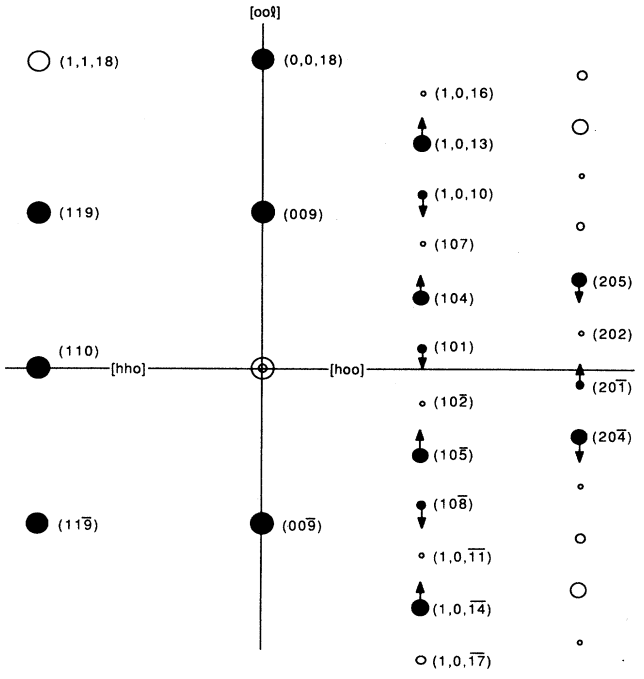

FIG. 3. The $\{h0l\}$ and $\{hhl\}$ planes of the ideal $9R$-phase reciprocal lattice of lithium and sodium metal. The sizes of the reciprocal-lattice spots qualitatively represent the strength of each reflection. The Miller indices for each reflection are to the right of each reciprocal-lattice spot. Solid spots indicate reflections observed and analyzed in the sodium diffraction data. The direction of the stacking-fault-induced shift of the reciprocal-lattice spots is shown with arrows.

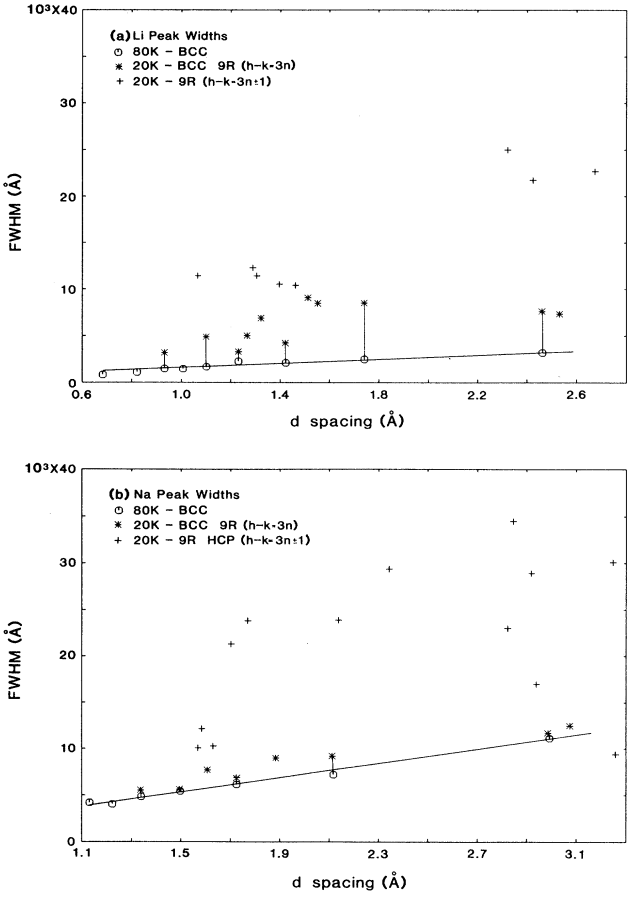

FIG. 4. The measured diffraction peak widths converted to Å for lithium and sodium metal before and after the martensitic transformation. The solid lines in the figure are linear least-squares fits to the 80-K-bcc linewidth data. The vertical lines in the figure connect bcc-phase diffraction peaks at 80 K before and at 20 K after the phase transformation. The figures show the additional broadening of the $9R$-phase diffraction lines that are affected by stacking faults. (a) Lithium metal at 80 and 20 K. (b) Sodium metal at 80 and 20 K.

been converted from TOF to d spacing using the appropriate conversion constants that characterize the spectrometer.[11,12] The uncertainty in the linewidth determination, as given by the standard deviation of the least-squares fits, is negligible. For both lithium and sodium, the 80- and 20-K linewidths of the bcc-phase diffraction lines have been connected with a vertical line. The widths of the lines at 80 K in both cases are very nearly the same as the instrumental width of the GPPD as measured by a silicon powder standard. Note that the resolution of the GPPD is different for the lithium and sodium data displayed because different detector banks (148° and 90°, respectively) have been used for the data analysis. In both metals at 20 K, the bcc-phase diffraction lines and the stacking-fault-unaffected $9R$-phase diffraction lines have similar linewidths. The solid lines shown in Figs. 4(a) and 4(b) are linear least-squares fits to the width of the 80-K bcc-phase diffraction lines.

The stacking-fault-affected $9R$-phase diffraction lines are grossly broadened. The broadening due to stacking faults alone was obtained by subtracting, in quadrature, the instrumental resolution as given by the fit to the 80-K linewidth data. The remaining broadening can be interpreted as a spreading of the line intensity profile along the c^* axis. The width of these diffraction lines, projected onto an $[h0l]$ line, has been tabulated in Table II.

For both metals, within experimental error, there is a strong correlation in the magnitude of the peak position shift and projected linewidth for the pair of lines observed at nearly the same d spacing [for example, the (104)-($10\bar{5}$) and the ($20\bar{4}$)-(205) pairs]. For the same peak family, the magnitude of the peak position shift and line broadening appears to increase as the length of the Q vector for that reflection increases. The $9R$-(101) and $9R$-($20\bar{1}$) diffraction peaks evidence considerably greater line broadening than any of the other $9R$-phase diffraction lines. It is also interesting that the peak position shifts in sodium are about 50% greater in magnitude than the ones observed in lithium metal.

B. Stacking-fault models

Stacking-fault-induced distortions of the diffraction pattern for a $9R$ lattice were calculated in detail by Monte Carlo methods in Ref. 6. Probability-tree difference-equation calculations of the effect of more complex stacking-fault defects in hexagonal and rhombohedral lattices have recently appeared in the literature.[15,16] In addition, theoretical discussions of the bcc to $9R$ transition in lithium[17] have predicted new transformation-induced defects in the low-temperature phase. For these reasons, it is appropriate to review the diffracted-intensity calculations for crystals with stacking-fault defects. This review will closely follow the development in Ref. 6. We will then show how the Monte Carlo calculations can be extended to the case of stacking faults in single crystals—the earlier calculations are strictly true only for powder specimens. A simple picture of the predicted line positions emerges that can be used to discuss the results of our powder-diffraction experiments and incorporate the single-crystal-diffraction results. Finally, we will compare the results of our model calculations with the effects observed in the diffraction data.

Starting with Eq. (10) from Ref. 6, the scattering cross section for a faulted hexagonal crystal along one of the reciprocal-lattice lines (h_0,k_0,l) can be written as

$$\frac{d\sigma}{d\Omega}(\mathbf{Q})=N_aN_b\delta(h-h_0)\delta(k-k_0)\times\sum_{m_3=-N_c}^{N_c}(N_c-|m_3|)Y_{m_3}(\mathbf{Q})\exp(-2\pi i m_3 l)\ , \tag{1}$$

where N_a and N_b are the number of unit cells in the crystal in the directions transverse to the c axis, and N_c is the number of layers in the c direction. The quantity $Y_{m_3}(\mathbf{Q})$ represents the "average structure-factor product" at a scattering vector $\mathbf{Q}=2\pi(h\mathbf{a}^*+k\mathbf{b}^*+l\mathbf{c}^*)$, i.e., the average over the crystallite of the product of the layer structure factors $F_n(\mathbf{Q})F^*_{n+m_3}(\mathbf{Q})$, for a distance m_3 layers apart. This form of the cross section for diffraction from stacking-fault-disordered crystalline materials was first derived by Wilson.[18] Berliner and Werner[6] demonstrated that it was a straightforward matter to obtain $Y_{m_3}(\mathbf{Q})$ by Monte Carlo techniques and that this method permitted easy construction and exploration of defect models.

Calculation of $Y_{m_3}(\mathbf{Q})$ proceeds from the observation that for a simple hexagonal lattice, each layer must be an A, B, or C layer and that the average structure-factor product is then given by

$$\begin{aligned}Y_{m_3}(\mathbf{Q})=&P_{AA}(m_3)F_AF_A^*+P_{AB}(m_3)F_AF_B^*+P_{AC}(m_3)F_AF_C^*+P_{BA}(m_3)F_BF_A^*+P_{BB}(m_3)F_BF_B^*\\&+P_{BC}(m_3)F_BF_C^*+P_{CA}(m_3)F_CF_A^*+P_{CB}(m_3)F_CF_B^*+P_{CC}(m_3)F_CF_C^*\ ,\end{aligned} \tag{2}$$

where $P_{AA}(m_3),P_{AB}(m_3),\ldots$ are the probabilities that two layers separated by a distance m_3 are of type A-A or A-B, ... For a powder, it is reasonable to assume that the probabilities of the occurrence of layer pairs AB, AC, BA, BC, CA, and CB are all equal. These probabilities are then $[1-p(m_3)]$, with $p(m_3)$ the probability that two layers separated by a distance m_3 are of the same type. When Eq. (3) is combined with the expressions for the values of the structure factors of monatomic hexagonal A, B, and C layers, one obtains a particularly simple expression for the average structure-factor product,

$$Y_{m_3}(h_0,k_0)=b^2\{p(m_3)+[1-p(m_3)]\times\cos[2\pi(h_0-k_0)/3]\}\ . \tag{3}$$

The quantity $p(m_3)$, calculated by Monte Carlo methods,[6] or, in some cases by probability-tree difference-equation methods,[15,16,19] can be used in Eq. (1) to obtain the diffracted intensity as a function of h,k, and l in reciprocal space. The intersection of the sphere of reflection with this reciprocal-lattice intensity distribution produces the diffracted intensity pattern for a powder specimen.

Measurements of the diffraction-line profiles of lithium single crystals below the martensitic transformation[7,8] initiated a reexamination of the calculation [Eqs. (1)–(3)]. For the case of stacking faults in a single crystal, the assumptions that allow the collapse of Eq. (2) into the simple form given by Eq. (3) are no longer valid. These assumptions are equivalent to assuming the presence of equal numbers of crystallites with the forward ($ABCBCACAB\ldots$) and the reverse ($BACACBCBA\ldots$) stacking order. In addition, for a faulted single crystal, one is no longer assured that the probability of the occurrence of A-B, A-C, B-A, B-C, C-A, and C-B pairs is equal or that there are equal numbers of A-A, B-B, and C-C layer pairs. Recalculation of the quantity $Y_{m_3}(\mathbf{Q})$ leads to a new expression for the diffracted intensity:

$$\frac{d\sigma(\mathbf{Q})}{d\Omega}=N_aN_b\delta(h-h_0)\delta(k-k_0)b^2\left[N_c+\sum_{m_3=1}^{N_c}2\{N_s(m_3)+[(N_c-m_3)-N_s(m_3)]\cos[2\pi(h_0-k_0)/3]\}\cos(2\pi m_3 l)\right.$$
$$\left.-\sum_{m_3=1}^{N_c}N_D\sin[2\pi(h_0-k_0)/3]\sin(2\pi m_3 l)\right] \tag{4}$$

with

$$N_S(m_3)=[N_{AA}(m_3)+N_{BB}(m_3)+N_{CC}(m_3)] \tag{5a}$$

and

$$N_D(m_3)=[N_{BA}(m_3)-N_{AB}(m_3)]+[N_{AC}(m_3)-N_{CA}(m_3)]+[N_{CB}(m_3)-N_{BC}(m_3)]\ . \tag{5b}$$

Here, $N_{AA}(m_3)$, $N_{BB}(m_3)$, and $N_{CC}(m_3)$ represent the number of A-A, B-B, and C-C layer pairs separated by a distance m_3 layers in the c direction and the quantities $N_{AB}(m_3)$, and $N_{AC}(m_3)$ are similarly defined.

The discussion of deformation faults and their effect on diffraction in Ref. 6 was based on the observation that any basal-plane layer in the $9R$ lattice can be viewed as hexagonal (H) if adjacent layers are of the same type or cubic (K) if adjacent layers are of a different type. The stacking order of the $9R$ crystal can then be denoted as $HKHHKHHKH\ldots$ instead of $ABCBCACAB\ldots$. Two distinct types of isolated deformation faults in the $9R$ lattice were identified: the $H\wedge H$ fault and the $H\wedge K$ fault. The first can be viewed as the result of a slip, perpendicular to the crystal c axis, between two layers that would have been $\ldots HH\ldots$ in the absence of the fault, and the second is formed by a slip between two layers denoted $\ldots HK\ldots$ or $\ldots KH\ldots$.

A more comprehensive roster of "nontwinning" stacking-fault defects in the $9R$ lattice has been compiled by Michalski and co-workers.[16] Consider the stacking sequence for the $9R$ lattice,

$$\ldots A_8B_9A_1B_2C_3B_4C_5A_6C_7A_8B_9A_1B_2\ldots$$
$$K\ H\ H\ K\ H\ H\ K\ H\ H\ K\ H\ H\ K\ .$$

Here we have numbered the positions of each layer in the stacking order and labeled each layer of the sequence, in terms of its neighbors, as hexagonal (H) or cubic (K) depending on its local environment. Introduction of a defect at layer 1 can result in the stacking

$$\ldots A_8B_9A_1C_3B_4C_5A_6C_7A_8B_9A_1B_2\ldots$$
$$K\ H\ K\ H\ H\ K\ H\ H\ K\ H\ H\ K$$

Following layer 1, the sequence continues with layer 3. We can refer to this defect as a (1,3) fault. In like fashion, it is possible to construct (1,4), (1,5), (1,7), and (1,9) fault sequences. Faults that occur following layer 2 result in a similar series of defects [(2,5), (2,6), (2,7), (2,8), and (2,1)] while those occurring after layer 3 give another set [(3,6), (3,8), (3,9), (3,1), and (3,2)]. Defects similarly constructed following sites 4-5-6 and 7-8-9 yield the same set of stacking sequences as sites 1-2-3.

The list of 15 defects formed in this manner are not all unique, and Table III contains the list of unique defects. The sequences are tabulated in H-K (Jagodzinski) notation;[20,21] they are further identified by the Zhdanov symbol used by Michalski,[16] the "construction" notation described above, and the stacking-fault identifications used by Berliner and Werner.[6]

In order to calculate the intensity distributions appropriate to random distributions of the stacking faults of Table III, we used Monte Carlo methods similar to the one previously described.[6] The Monte Carlo program uses an ensemble of randomly faulted crystallites to compute the diffracted intensity for each of the fault types along a $[10l]$ line in reciprocal space. Note that the $\sin[2\pi(h_0-k_0)/3]$ term in Eq. (4) reverses the direction of the diffraction-line-peak shifts when the intensity distribution is calculated for the $[20l]$ reciprocal-lattice line. These calculations are in complete agreement with the previous Monte Carlo results for the $H\wedge K$, $K\wedge H$, $H\wedge H$, and β faults[6] and are in qualitative agreement with the analytic estimates of peak shifts obtained by Michalski *et al.*[16] and Lele.[19]

TABLE III. Stacking-fault stacking sequences for nontwinning fault types in the 9*R* lattice. The fault types are identified with the Zhdanov symbol used by Michalski *et al.* (Ref. 15), the deformation fault notation of Ref. 6, and the "construction notation" used in this work.

Zhdanov symbol	Stacking sequence	Fault type	Deformation growth type
2(3)	*K H H K H K K H K H H K*	(1,3)	
1(3)	*K H H K H H K K H H K H*	(1,4) (2,5) (3,6)	β
1(21)	*K H H K H K H H H K H H*	(1,5)	$H \wedge K$
2(2)	*K H H K H K H K H H K H*	(1,7) (3,9)	
1(1)	*K H H K H H H H K H H K*	(1,9) (2,1) (3,2)	
2(12)	*K H H K H H H K H K H H*	(2,6)	$K \wedge H$
1(4)	*K H H K H H K K K H H K*	(2,7) (3,8)	
1(111)	*K H H K H H H H H H K H*	(2,8)	
1(5)	*K H H K K K K H H K K K*	(3,1)	$H \wedge H$

Qualitative agreement with the experimental results for lithium and sodium metal is obtained for the fault denoted by (1,9) in the "construction" notation. The intensity distribution calculated for a 10% per-layer occurrence probability of these faults is shown plotted along a [10*l*] reciprocal-space line in Fig. 5(a). The distribution corresponding to a 200-layer perfect crystal is shown in Fig. 5(b). The shift of the peak position for the 9*R*-(104) (toward $+l$) and the 9*R*-(101) (toward $-l$) are in qualitative agreement with the data and it is especially interesting that the 9*R*-(107) is grossly broadened. This is very likely the reason that none of the (107)-type peaks are observed in the powder data and are very weak in the single-crystal diffraction data.[7,8,13]

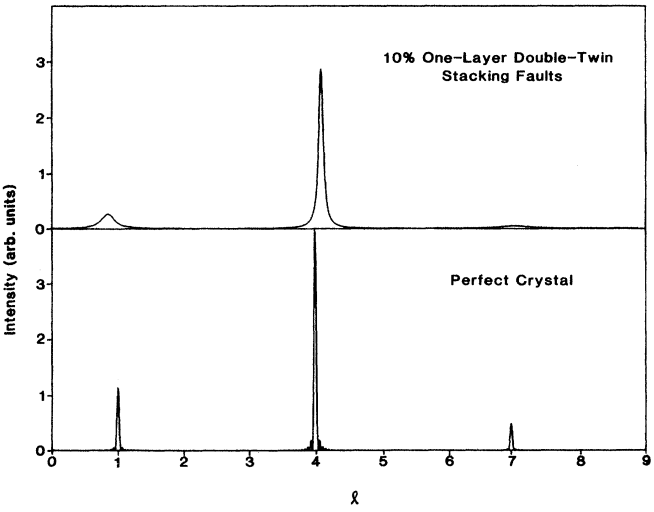

FIG. 5. Calculated reciprocal-space intensity distributions for a 9*R* crystal calculated by Monte Carlo methods from an ensemble of 10 000 crystallites each 200 layers long in the *c* direction. (a) The distribution corresponding to a 10% random distribution of one-layer double-twin stacking faults. (b) The intensity distribution for a 200-layer crystal without stacking faults.

This stacking fault may be considered as a one-layer double-twin defect. At the fault, the stacking sequence reverses, goes backwards for one layer, then proceeds forward again. It is similar to the multilayer double-twin stacking faults postulated in recent theoretical work on the bcc to 9*R* transformation in lithium metal.[17] There, it was suggested that these multilayer defects might arise from the breaking of the space-group symmetry of the bcc phase by the presence of a defect. We have calculated the diffracted intensity distributions for random introduction of multilayer double-twin defects in the stacking sequence of a 9*R* lattice. For these defects, the stacking sequence reverses at a fault, proceeds in the reverse direction for several layers, and then reverses again. If the number of reverse stacking layers is large enough, the "twin" reflections ($-h+k-l=3n\pm1$) appear in the calculated intensity distributions. The single-crystal diffraction results for both lithium and sodium metals show no evidence of these twin reflections.[7,8,13] For a smaller number of reversed stacking layers, we were unable to obtain calculated peak position shifts of the (104)-type peaks coupled with the extreme broadening of the (107)-type peaks which are in qualitative agreement with the lithium and sodium diffraction data.

Figure 6(a) shows the diffraction peak position shift, in units of *l*, as a function of the density of one-layer double-twin stacking faults. Note that the direction of the peak position shift of the 9*R*-(101) is toward $-l$, opposite to that of the (104) and (107). These peak-

TABLE IV. The results from least-squares fits to the diffraction peak position shifts and diffraction peak broadening given by the Monte Carlo calculations of one-layer twin faults in 400-layer 9*R* crystallites. The values for the peak shift or peak width can be found by multiplying the appropriate value in the table by the per-layer fault probability.

h k l	Peak shift	Peak width
1 0 1	−1.553	2.301
1 0 4	0.919	0.635
1 0 7	0.628	6.594

position-shift calculations are in essential agreement with the results of Michalski *et al.*[16,22] The differences are presumably due to the approximations required to obtain the probability-tree difference-equation solutions. The Monte Carlo results for the full width at half maximum (FWHM) of the 9*R* diffraction peaks are shown in Fig. 6(b) in units of *l* as a function of the stacking-fault probability. Our calculated diffraction peak widths are different from those of Ref. 16 which predict substantially greater peak broadening.

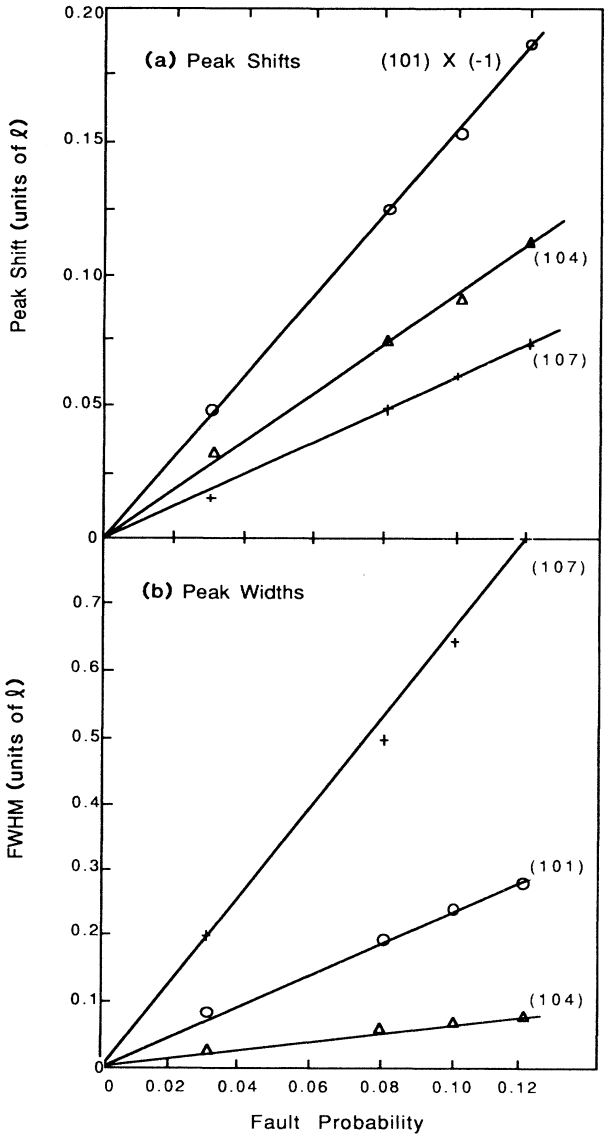

FIG. 6. The diffraction peak position shifts and diffraction peak widths, in units of *l*, calculated for one-layer twin faults as a function of the stacking-fault probability. The points in the figure are the result of Monte Carlo calculations using 10 000 400-layer crystallites at each fault probability. The solid lines are linear least-squares fits to the Monte Carlo results for the stacking-fault-induced peak position shift and peak width. Note that the peak position shift for the 9*R*-(101) peak is negative. (a) Peak position shifts. (b) Diffraction peak widths.

Figures 6(a) and 6(b) illustrate the strong shift of the (101)-type diffraction peaks and the unusually strong broadening of the (107)-type peaks that appear in the lithium and sodium diffraction data. The lines in the figure are linear least-squares fits to the Monte Carlo–calculation results. A summary of the parameters from these fits is in Table IV. On the basis of these calculations, it is possible to estimate the stacking-fault density that produces the observed peak shifts. In lithium metal, we obtain a stacking-fault occurrence probability of 6.3% (per layer) based on the average shift of the 9*R*-phase (104)-($10\bar{5}$) peak pair. In sodium metal, the fault density is estimated at 9.3% per layer by the same method. The peak width broadening for the (104)-($10\bar{5}$) diffraction peaks of lithium is then predicted to be 0.051, in units of *l*, which is substantially different from the measured average of value 0.120. Similar, although smaller, discrepancies are obtained for the peak widths of the sodium (104)-($10\bar{5}$) diffraction peaks based on the estimate of 0.093 probability of one-layer twin faults.

IV. SUMMARY AND CONCLUSIONS

We have obtained neutron powder-diffraction data for lithium and sodium metals at 80 K before the martensitic transformation and at 20 K, after the phase transformation. We have also obtained high-resolution neutron powder-diffraction patterns for potassium metal at 80 and 10 K. We show that the phase transformation in sodium and lithium metal is to a hexagonal polytype form, the 9*R* crystal structure. In lithium metal, we find that 66% of the material transforms to the new phase. This is very similar to the 70% transformed fraction measured by Berliner and Werner.[6] In sodium metal, we find the transformed fraction to be 43%. This is comparable to the value determined by Barrett[2] for the hexagonal fraction in heavily cold-worked sodium although much larger than the transformed fraction for specimens that were simply cooled below the transformation temperature. In potassium metal, to the limit of sensitivity of the experiment (4%), no transformation was observed. Our measurements indicate that lithium undergoes a 0.09% volume expansion during the martensitic transformation, while in sodium metal, the atomic volume expansion is 0.3%. The low-temperature diffraction patterns for lithium and sodium evidence peak position shifts and broadening that are characteristic of diffraction from crystals with stacking-fault defects. These peak position shifts are incompatible with the presence of large densities of $H \wedge K$ and $K \wedge H$ simple deformation faults.

We have extended the Monte Carlo–calculation methods of Ref. 6 to determine the effect of stacking faults on diffraction from single crystals and used these results to analyze our powder-diffraction data. Our calculations for a series of "nontwinning" stacking-fault defects demonstrates that only one of these, the one-layer double-twin stacking fault is compatible with the data.

This defect results in the appropriate diffraction peak position shifts: the $9R$-(104) shifts to longer d spacing $(+l)$ while the $9R$-(101) moves to smaller d spacing $(-l)$. This defect is furthermore shown to severely broaden the $9R$-(107)-type lines. These lines are absent in the powder data even though one would normally expect them to be clearly visible. The stacking-fault probability after the martensitic transformation is estimated at 0.063 (per layer) for lithium metal on the basis of the peak position shift of the (104-($10\bar{5}$) diffraction peaks. In sodium metal, a similar analysis leads to an estimate of a 0.095 stacking-fault probability. The identification of this defect is in gratifying agreement with recent theoretical analyses of the mechanism of the structural transformation in lithium.[17] It is reasonable to relate the greater stacking-fault density in sodium to the appearance of an hcp phase, in addition to the $9R$ phase, and to its larger transformation-induced volume change.

It would be preferable to perform a complete fit to the diffraction pattern, including the shifts of peak positions as they are predicted by the model of the one-layer double-twin stacking fault. Such an analysis was performed in Ref. 6 for simple deformation faults. We have found that the data from this experiment is subject to preferred orientation effects, making it unproductive to attempt this line of investigation. To confirm this stacking-fault model in detail, it will be necessary to study the diffracted intensity distributions from single-crystal specimens along the appropriate lines in reciprocal space.

The diffraction data for sodium suggest the presence of a hcp phase with stacking-fault-type peak-position displacement and peak width broadening. Clear evidence of a hcp phase is present in single-crystal neutron-diffraction data.[13] We have not attempted to analyze the nature of the hcp-phase defects in detail since too few of the hcp diffraction peaks are visible in our data. The presence of this phase is, however, particularly interesting in view of the recent results from diffraction experiments on lithium metal under hydrostatic pressure: the specimen was observed to transform from a mixed bcc-$9R$ form to a mixed fcc-bcc form on warming from 70 K at 6.5 kbar.[23] The fcc phase appears to have a small or negligible density of stacking faults. Finally, this experiment shows that the defect structure in lithium and sodium metal after the martensitic transformation is the same in our extruded-wire polycrystalline specimens as it is for well-annealed single-crystal specimens.

The variation observed in the magnitude of the peak position shift and diffraction-line broadening for peaks of the same "family" such as the $9R$-(104) and the $9R$-(10,13) is, as yet, not understood. The additional broadening of the diffraction peaks, over that predicted by the stacking fault model, and the extreme broadening of the $9R$-(101) and $9R$-($20\bar{1}$) are similarly unexplained. It is reasonable to assume that these effects are most probably due to additional transformation-induced defects in the martensite phase. The substantial qualitative and quantitative agreement between the experimental data and the one-layer twin-fault model calculations supports the phenomenological analysis of this phase transformation.[17] It also makes easier the identification of the residual defects in these two important martensite examples.

ACKNOWLEDGMENTS

The authors wish to acknowledge the substantial help and assistance of the Intense Pulsed Neutron Source, Argonne National Laboratory (Argonne, IL) (ANL-IPNS) scientific staff. In particular, the authors would like to thank F. Rotella, J. Faber, and J. Carpenter for help with calculations and for many extremely useful discussions on the interpretation of TOF powder-diffraction data. The authors would also like to thank F. Ross of the University of Missouri Research Reactor (Columbia, MO) (MURR), A. Krawitz and S. A. Werner of the University of Missouri, and R. Gooding of Cornell University for their suggestions and criticism. The authors also thank S. A. Werner for the sodium metal used as a specimen in preliminary diffraction experiments. This work has benefited from the use of the ANL-IPNS. This facility is funded by the U.S. Department of Energy, Basic Energy Sciences (BES)-Materials Science, under Contract No. W-31-109-Eng-38.

[1]C. S. Barrett and O. R. Trautz, Trans. Am. Inst. Min. Metall. Pet. Engr. **175**, 579 (1948).
[2]C. S. Barrett, Acta Crystallogr. **9**, 671 (1956).
[3]C. M. McCarthy, C. W. Tompson, and S. A. Werner, Phys. Rev. B **22**, 574 (1980).
[4]A. W. Overhauser, Phys. Rev. Lett. **53**, 64 (1984).
[5]A. H. Danne, R. E. Rundle, H. G. Smith, and F. H. Spedding, Acta Crystallogr. **7**, 532 (1954).
[6]R. Berliner and S. A. Werner, Phys. Rev. B **34**, 3586 (1986).
[7]H. G. Smith, Phys. Rev. Lett. **58**, 1228 (1987).
[8]H. G. Smith and R. Berliner (unpublished).
[9]Alpha Products, P.O. Box 299, 152 Andover St., Danvers, Massachusetts, 01923.
[10]J. D. Jorgensen, J. Faber, Jr., J. M. Carpenter, R. K. Crawford, J. R. Haumann, R. L. Hitterman, R. Kleb, G. E. Ostrowski, F. J. Rotella, and T. G. Worlton, J. Appl. Crystallogr. **21**, 321 (1989).
[11]F. J. Rotella, User's Manual for Rietveld Analysis of Time-of-Flight Neutron Diffraction Data at IPNS, Argonne National Laboratory IPNS Internal Document, 1982.
[12]J. Faber, Jr. and R. L. Hitterman, *Advances in X-Ray Analysis 29*, edited by C. S. Barrett *et al.* (Plenum, New York, 1986), p. 119.
[13]R. Berliner, H. G. Smith, J. Copley, and J. Trivisonno (unpublished).
[14]S. A. Werner (private communication).
[15]E. Michalski, Acta Crystallogr. Sect. A **44**, 640 (1988).
[16]E. Michalski, S. Kaczmarek, and M. Demianiuk, Acta Crystallogr. Sect. A **44**, 650 (1988).
[17]R. Gooding and J. Krumhansl, Phys. Rev. B **38**, 1695 (1988).
[18]A. J. C. Wilson, Proc. R. Soc. London, Ser. A **180**, 277 (1941).
[19]S. Lele, Acta Crystallogr. Sect. A **30**, 689 (1974).

[20]A. R. Verma and P. Krishna, *Polymorphism and Polytypism in Crystals* (Wiley, New York, 1966).
[21]H. Jagodzinski, Acta Crystallogr. **2**, 201 (1949).
[22]In this work, the fault-occurrence probability is the probability per layer. To use the formulas in Ref. 15, multiply this number by 2.
[23]H. G. Smith, R. Berliner, and J. D. Jorgensen, Physica B **156-157**, 53 (1989).